Nanoscale

Accepted Manuscript

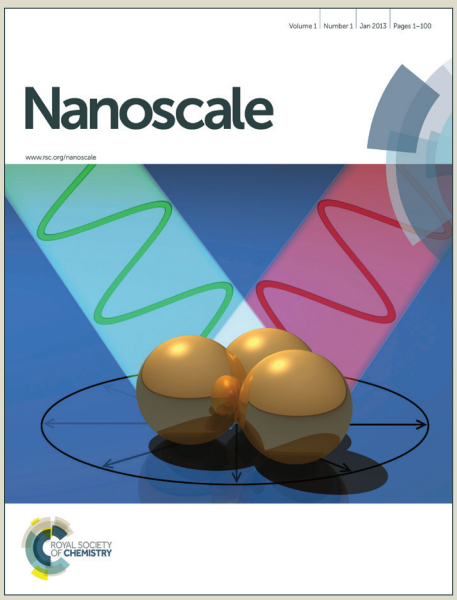

ROYAL SOCIETY OF CHEMISTRY

www.rsc.org/nanoscale

Efficient Solution-Processed Small-Molecule Solar Cells by Insertion of Graphene Quantum Dots

Dong Hwan Wang, *[a] Jung Kyu Kim,[b] and Jong Hyeok Park,[b]

Received (in XXX, XXX) Xth XXXXXXXXX 200X, Accepted Xth XXXXXXXXX 200X
First published on the web Xth XXXXXXXXX 200X
DOI: 10.1039/b000000x

In this work, we have been demonstrated the results of several positive effects that arise from the addition of graphene quantum dots (GQDs) to solution-processed small molecule bulk-heterojunction (SM-BHJ) solar cells fabricated from a p-DTS(FBTTh$_2$)$_2$/[6,6]-phenyl C_{71} butyric acid methyl-ester ($PC_{71}BM$). The device with an optimized ratio of GQDs exhibits increased current density and fill factor which correlate an 10% improved external quantum efficiency (EQE) and induce a favorable SM-BHJ morphology. Additionally, the multiple scattering of the GQDs in the SM-BHJ leads to longer optical path lengths according to the analysis of diffuse reflectance spectra and UV/Vis absorption spectra. The GQDs inserted SM-BHJ film with optimized concentration exhibits decreased charge transport resistance significantly by impedance measurements with effective charge extraction at the device which contribute to 15% enhancement of power conversion efficiency (PCE).

Introduction

Sp^2-hybridized carbon based nanomaterials (nanocarbons) have attracted considerable attention owing to their low cost, outstanding electronic and mechanical properties, and chemical stability.[1] The sufficient conjugation and p-orbitals in the nanocarbons can result in advantageous characteristics, including excellent high carrier mobility,[2-4] the quantum hall effect,[5-10] the ambipolar electric field effect,[1] and massless Dirac fermions.[11] As a promising 2D nanocarbon, graphene has been widely exploited for electronic device applications due to its high conductivity in a ~3.4 Å thick ultrathin monolayer.[12-13] However, the ambipolar field effect and the zero band gap property make it difficult to use graphene for opto-electric devices. Especially, the excellent carrier mobility, the ultrathin thickness, and high transmittance of graphene film are considered as the most interesting properties for photovoltaic devices because the solar to power conversion efficiency (PCE) is strongly influenced by the charge carrier transport characteristics from the active layer to both electrodes.[14-15] However, the zero band gap property of graphene has been considered as a limiting factor for light harvesting performance in photovoltaic cells; nevertheless, a monolayer graphene can absorb less than 2.5% incident light, which is analogous to some of the small molecular aromatic rings, due to the extinction coefficient of $10^5 M^{-1}cm^{-1}$.[16]

In order to tune the band gap and band edges in graphene, a nanostructure modification of graphene based materials has been conducted using by lithography, carbonization, and hydrothermal synthesis.[17-19] By controlling the size, shape, and functionalities, not only the band gap energy but also the electron affinity and the carrier mobility of graphene based nanostructures was modified. Interestingly, 0-dimensional graphene quantum dots (GQDs) show significantly attractive features for the optoelectronic devices among the graphene based nanocarbons.[20] Because of the quantum confinement effect and the sp^3 hybridized carbons on the sides of the edges, GQDs can possess a tunable band gap energy as well as electronic transition induced by the energy gaps between π and π* or n and π*.[21-22] Furthermore, by tailoring the ionization potential and the electron affinity of GQDs, the charge carrier conductance of the optoelectronic devices can be easily tuned.[20,23-24]

Recently, significant approaches have been taken to introduce GQDs into bulk heterojunction (BHJ) organic photovoltaics (OPVs). Owing to their considerable potential for flexible photovoltaics and large-scale mass production based on a roll-to-roll process, OPVs have been considered as a promising next-generation solar cell.[25-29] However, the poor carrier mobility of the organic semiconductors restrains the BHJ film thickness caused by the undesired charge recombination, thereby resulting in an insufficient light harvesting performance.[30-31] Due to the efficient charge carrier conductance and the balanced light absorptivity of GQDs, high-efficiency polymer solar cells were achieved. In addition, the superb carrier transport property of GQDs induced a decrease in the series resistance when GQDs were used as electron or hole extraction layers in the organic solar cells.[32-33]

Here, we report the results of a study that demonstrates several positive effects that arise from the addition of GQDs to solution-processed small molecule based BHJ solar cells fabricated from p-DTS(FBTTh$_2$)$_2$/[6,6]-phenyl C71 butyric acid methyl-ester ($PC_{71}BM$). The small molecule donor of p-DTS(FBTTh$_2$)$_2$ is a very promising material which has low molecular weight batch-to-batch variation during synthesis, good solubility in organic solvent, and high performance due to efficient electron withdrawing functionality, as revealed in previous researches.[34-36] The GQDs were synthesized using a deoxidization method with a hydrothermal reduction with oxidized grapheme oxide (GO), as reported previously.[22]

Experimental

Synthesis of GQDs: The synthesis steps of GQDs were followed by the [Ref. 22] in Experimental Section.

Device Fabrication: ITO-coated glass substrates were cleaned in detergent, deionized water, acetone, and isopropanol during ultra-sonication. The hole transport layer of PEDOT:PSS (AI 4083) was spin-cast at 5000 rpm for 40 s with the film thickness of ~35

nm after the treatment of UV ozone (20 min). The BHJ blended solution was prepared by p-DTS(FBTTh$_2$)$_2$:PC$_{71}$BM with an overall concentration of 35 mg/ml (Donor : Acceptor = 60 : 40 weight ratio) in chlorobenzene with 0.4 v/v% of diiodooctane (DIO) solvent additive. The BHJ solution was stirred at 500 rpm on top of a 60 °C hotplate overnight, and the prepared solution was annealed at 90 °C for 15 min before spin-coating. The BHJ active layer thickness was ~120 nm. The films were then heated at 80 °C for 10 min to dry the solvents. Finally, a Ca/Al cathode with a thickness of ~ 20 nm/100 nm was thermally deposited under 4 × 10^{-6} Torr using an evaporator.

Characterization: The light source was calibrated using silicon reference cells with an intensity of 100 mW/cm^2 of an AM 1.5 Global solar simulator. The *J-V* characteristics of the single and tandem solar cells were measured using a Keithley 236 source unit. All the cell areas were 11.76 mm^2 as determined by the aperture for accurate measurement. The EQE was measured after monochromatic power calibration using a QE measurement system (PV measurements, Inc.).

Other characterization methods: The XPS and the FT-IR spectra were obtained using a VG Multilab ESCA 2000 system with a twin-anode Mg/Al kα and a Bruker IFS-66/S spectrometer, respectively. The AFM images of GQDs were taken in noncontact mode using a Seiko SPA-300HV. The TEM images were measured using a JEOL JEM ARM 200F at 200 KV. Film topography images were obtained using an AFM (Veeco diINNOVA 840-012-711, tapping mode). Impedance spectroscopy measurement was conducted by using a potentiostat (CH Instruments, CHI 660) under AM 1.5G 1 sun light illumination from the solar simulator.

Results and discussion

Property of graphene quantum dots (GQDs) and performances of small-molecule solar cells with GQDs

As shown in Figure 1, the average thickness and diameter of the GQDs were ~1.5 nm and ~5 nm, respectively. Owing to the availability of sufficient oxygen-related functional groups, GOs were composed of sp^2 and sp^3 hybridization.

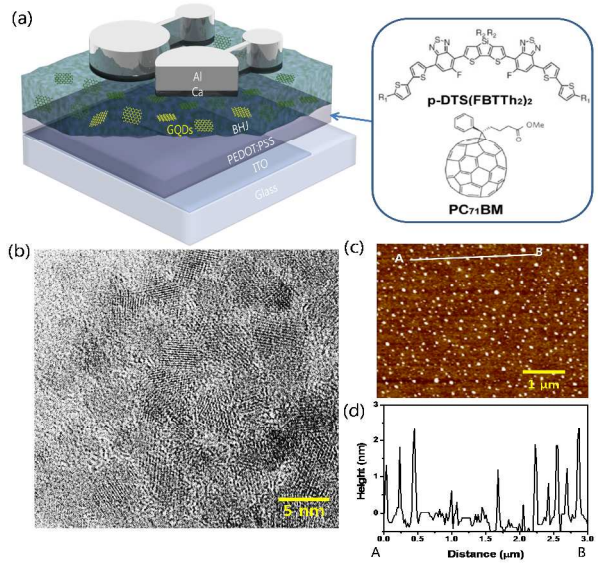

Figure 1. (a) Schematic illustration of the GQDs embedded BHJ solar cell, (b) high resolution transmission electron microscopy (TEM) image, (c) atomic force microscopy (AFM) image, and (d) height profiling curve from A to B in the AFM image of GQDs.

However, during an oxidization and hydrothermal reduction process, oxygen atoms in the functionalities were steadily reduced resulting in the recovery of sp^2 carbons in the GQDs. The inset of Figure 1 shows the molecular structure of p-DTS(FBTTh$_2$)$_2$, PC$_{71}$BM, and the device sequential structure. The HOMO and LUMO energy levels of p-DTS(FBTTh$_2$)$_2$ are 5.12 and 3.34 eV, respectively.[31]

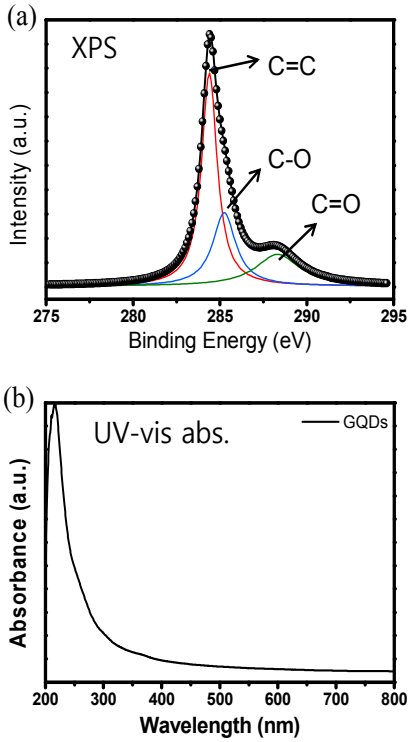

Figure 2. (a) X-ray photoelectron spectra (XPS) and (b) UV-visible absorbance of GQDs.

In Figure 2(a), the X-ray photoelectron spectra (XPS) shows that sp^2 carbons (C=C, at 284.5 eV) are dominant in the GQDs, whereas the hydroxyl (C-O, at 286.0 eV) and carbonyl or carboxyl (C=O, at 288.0 eV) carbon peaks are less weak. As shown in Figure 2(b), the GQDs exhibit a weak UV/Vis absorption intensity through the visible ranges. Fourier transform infrared spectroscopy (FT-IR) also exhibits the property of the sp^2 carbons and the functional groups are shown in Figure S1. In order to incorporate into the BHJ solution, the synthesized GQDs were dispersed in cholorobenzene solvent by 0.5 ~ 2 wt. %. Due to the hydrothermal reduction process using the deoxidization method, GQDs could be well dispersed into the organic solvent so that GQDs has sufficient sp^2 hybridized carbons. The GQDs solution was mixed with the BHJ solution with various weight ratios; the mixture solution was then spin cast on top of the PEDOT:PSS film coated ITO glass.

Figure 3(a) exhibits the *J-V* characteristics of the p-DTS(FBTTh$_2$)$_2$:PC$_{71}$BM BHJ devices fabricated without and with GQDs (0.5 ~ 2 wt. %) under AM 1.5G irradiation at 100 mW/cm^2. The efficiency parameters are summarized in Table 1.

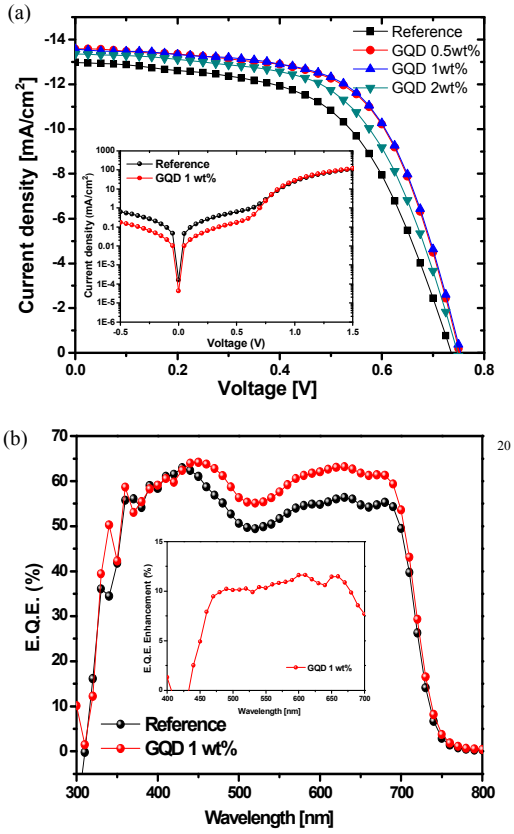

Figure 3. (a) *J-V* characteristics and (b) EQE of the p-DTS(FBTTh$_2$)$_2$:PC$_{71}$BM BHJ devices fabricated without and with GQDs (0.5 ~ 2 wt. %) under AM 1.5G irradiation at 100 mW/cm^2 (v/v). Inset figure (a) and (b) show the dark current of the devices fabricated without and with GQDs and EQE enhancement, respectively.

The reference cell with pristine p-DTS(FBTTh$_2$)$_2$:PC$_{71}$BM BHJ has PCE = 5.42% with J_{SC} = 12.98 mA/cm^2, V_{OC} = 0.736 V, and a fill factor (FF) of 57%. To characterize the performance of pristine BHJ and BHJ with GQDs, the additional interlayer is not deposited between BHJ and the Al cathode. When the device fabricated by the insertion of GQDs with a weight ratio of 0.5%, the V_{OC}, J_{SC}, and FF increase to 0.752 V, 13.58 mA/cm^2, and 62%, respectively. The optimum ratio of 1 wt. % GQDs in BHJ of p-DTS(FBTTh$_2$)$_2$:PC$_{71}$BM provided the best efficiency: PCE = 6.40% with a J_{SC} = 13.57 mA/cm^2, V_{OC} = 0.754 V, and a fill factor (FF) of 63% compared to the device with 2 wt. % GQDs: PCE = 5.94% with a J_{SC} = 13.35 mA/cm^2, V_{OC} = 0.748 V, and a fill factor (FF) of 60%. These results reveal that the most positive effects and best concentration of GQDs occurred in BHJ, as confirmed by our previous original researches.[37-39] Especially, the FF and J_{SC} of small molecule based BHJ solar cells with GQDs exhibit increased values from 57% to 63%, and 12.98 to 13.58 mA/cm^2, respectively, as shown in Table 1. The external quantum efficiency (EQE) was obtained from the BHJ devices without and with GQDs from Figure 3(b). The EQE value shows a similar intensity of 60% at the wavelength of 400 nm, while the increased EQE was detected with a 10% average enhancement (see inset figure) for the device fabricated with an optimized 1wt. % of GQDs in small molecule BHJ film. Figure S2 exhibits the UV/Vis absorption spectra of the BHJ film without (pristine) and with GQD (1 wt. %). Thus, the enhanced J_{SC} is originated from the improved absorption and increased EQE.

p-DTS(FBTTh$_2$)$_2$:PC$_{71}$BM	V_{OC} [V]	J_{SC} [mA/cm^2]	FF [%]	PCE [%]
Pristine BHJ	0.736	12.98	57	5.42
GQD - 0.5 wt.%	0.752	13.58	62	6.36
GQD - 1 wt.%	0.754	13.57	63	6.40
GQD - 2 wt.%	0.748	13.35	60	5.94

Table 1. Efficiency parameters of solar cells based on p-DTS(FBTTh$_2$)$_2$:PC$_{71}$BM BHJ fabricated without and with GQDs (0.5 ~ 2 wt. %).

Analysis of small-molecule based BHJ with GQDs: morphology, reflectance, and charge transport resistance

To characterize the morphological changes depending on the GQDs in small molecule based BHJ, an atomic forced microscopy topography (AFM) analysis was conducted.

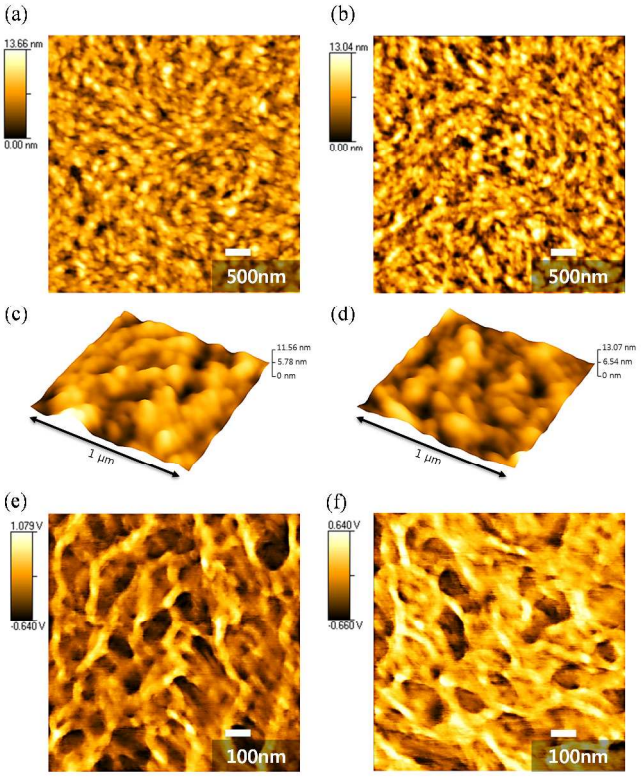

Figure 4. AFM 2D topography (a) and (b), and 3D (c) and (d) images of BHJ films w/o. or w. GQDs, respectively. (e) and (f) AFM topography phase images of (C) and (D).

In Figures 4(a) and (b), AFM images show that the BHJ layers with or without GQDs are uniformly coated on the PEDOT:PSS layer without any harmful cracks. However, significant changes in morphology resulted from the 2D based QD structure of the GQDs incorporated in the BHJ layer. As shown in the 3D AFM topography images in Figures 4(c) and (d), the donor-acceptor (D-A) phase separation shape changed by incorporating GQDs. The peaks of the domains in the GQD incorporated BHJ film had softened considerably, and the distance between the peaks increased more than the bare BHJ film. This is because the QD structure of the GQDs of 5 nm diameter and 2 nm thickness can have an influence on the morphology since the D-A phase separation distance was less than 20 nm. Furthermore, the distribution of dark and bright regions in the topography phase images shown in Figures 4(e) and (f) exhibit effective surface morphology of the GQDs incorporated BHJ film compared to the pristine BHJ film due to the smaller height variation of surface morphology. Hence, the favorable morphology and phase separation of the BHJ film in terms of the well dispersed GQDs induced an enhanced current density with high carrier conductivity and possibly efficient light absorptivity through the BHJ domains, thereby affecting not only the resistance parameters but also improving light harvesting at the BHJ solar cells.

Furthermore, the increased current density with (enhanced EQE) implies that more light is harvested in the small molecule BHJ film because of possibly multiple reflection from light scattering by the GQDs. We could neglect the surface plasmon resonance (SPR) effect on the GQDs from the optical simulation of the E-field intensity distribution of the GQD obtained by the finite difference time domain (FDTD) method in Figure S3.[37] Thus, the improvements of the EQE, particularly related to the dominant light scattering and improved charge carrier harvesting efficiency. To confirm the role of GQDs in small molecule BHJ film, we measured the diffuse reflectance spectra as shown in Figure 5(a). Consequently, the smaller reflection at the device with GQDs indicates the higher light absorptivity of the incident light.

In order to understand the charge transport resistance for the BHJ layer, Nyquist plots were conducted by electrochemical impedance spectroscopy measurement and Z-View software as shown in Figure 5(b). Because the GQDs device and reference device had the same device structure, that of ITO/PEDOT:PSS/ BHJ/Al, the ohmic resistance values, which were strongly related to the interface resistance of both electrodes (anode and cathode), were similar: 53.2 Ω for the GQDs device, and 54.0 Ω for the reference device. Moreover, the similar shape and size of the lower resistance region of the semicircles for both devices implied that there were no differences in the interlayers, and the interfaces between BHJ and the interlayer. However, the charge transport resistance in the BHJ layer with GQDs was significantly decreased by around 2 times, compared with the reference values (of 6050 Ω for the GQDs device, and 12089 Ω for the reference device). Due to the outstanding charge conductance of GQDs,[22] the charge transport resistance in the GQDs embedded small molecule based BHJ layer was significantly reduced, thereby enhancing the charge separation and extraction performance in the active layer.

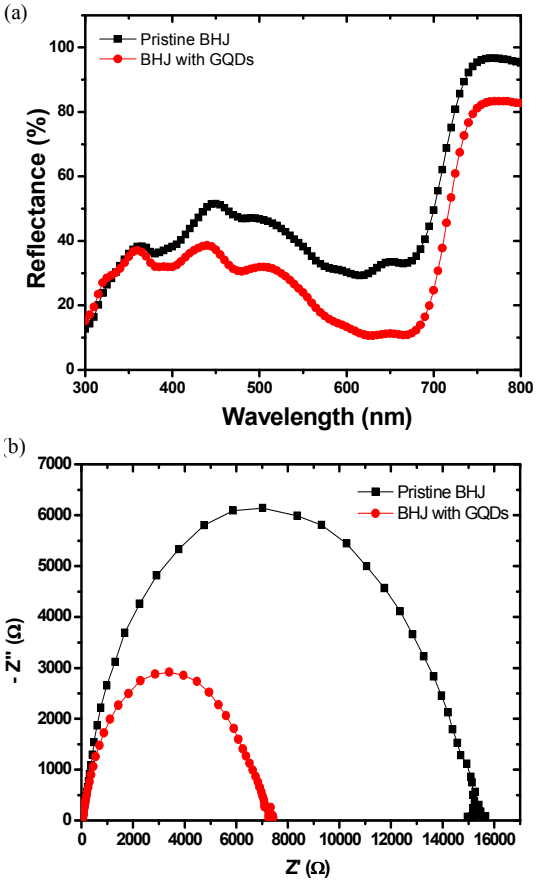

Figure 5. (a) Diffuse reflectance spectra of the devices fabricated with pristine p-DTS(FBTTh$_2$)$_2$:PC$_{71}$BM BHJ (black curve) and BHJ with the addition of 1 wt. % GQDs (red curve) (b) Nyquist plots of electrochemical impedance spectroscopy at open circuit voltage (1 wt. % of GQDs was incorporated into small-molecule based BHJ film).

Conclusions

In conclusion, we demonstrated the high performance solution-processed small molecule BHJ solar cells by the insertion of GQDs for the first time. The GQDs play an important role of increased J_{SC} and FF at the device due to inducing favorable BHJ morphology and improved EQE. Furthermore, the multiple scattering of the GQDs in BHJ leads to longer optical path lengths which give rise to improved light absorption by analysis of diffuse reflectance spectra. The GQDs inserted small molecule based BHJ film also exhibits significantly reduced charge transport resistance from the impedance spectroscopy measurement. The combination of those factors: improved light absorption and effective charge conductor lead to a high

efficiency solution processed small molecule solar cells.

Acknowledgements

This research was supported by the Basic Science Research Program through the National Research Foundation of Korea (NRF), funded by the Ministry of Science, ICT & Future Planning (2014R1A1A1002419).

Notes and references

[a]*School of Integrative Engineering, Chung-Ang University, 84 Heukseok-ro, Dongjak-gu, Seoul 156-756, Republic of Korea; E-mail: king0401@cau.ac.kr*
[b]*School of Chemical Engineering and SAINT, Sungkyunkwan University, Suwon 440-746, Republic of Korea*

1. K. S. Novoselov, A. K. Geim, S. V. Morozov, D. Jiang, Y. Zhang, S. V. Dubonos, I. V. Grigorieva, A. A. Firsov, *Science* 2004, **306**, 666
2. K. I. Bolotin, K. J. Sikes, Z. Jiang, M. Klima, G. Fudenberg, J. Hone, P. Kim, H. L. Stormer, *Solid State Commun*. 2008, **146**, 351.
3. K. S. Novoselov, A. K. Geim, S. V. Morozov, D. Jiang, M. I. Katsnelson, I. V. Grigorieva, S. V. Dubonos, A. A. Firsov, *Nature* 2005, **438**, 197.
4. S. V. Morozov, K. S. Novoselov, M. I. Katsnelson, F. Schedin, D. C. Elias, J. A. Jaszczak, and A. K. Geimet, *Phys. Rev. Lett.* 2008, **100** 016602.
5. K. S. Novoselov, E. McCann, S. V. Morozov, V. I. Fal'ko, M. I. Katsnelson, U. Zeitler, D. Jiang, F. Schedin, A. K. Geim, *Nat. Phys.* 2006, **2**, 177.
6. Z. Jiang, Y. Zhang, Y.-W. Tan, H.L. Stormer, P. Kim, *Solid State Comm*. 2007, **143**, 14.
7. Z. Jiang, Y. Zhang, H. L. Stormer, P. Kim, *Phys. Rev. Lett*. 2007, **99**, 106802.
8. Y. Zhang, Y.-W. Tan, H. L. Stormer, P. Kim, *Nature* 2005, **438**, 201.
9. K. S. Novoselov, Z. Jiang, Y. Zhang, S. V. Morozov, H. L. Stormer, U. Zeitler, J. C. Maan, G. S. Boebinger, P. Kim, A. K. Geim, *Science* 2007, **315**, 1379.
10. B. Ozyilmaz, P. Jarillo-Herrero, D. Efetov, D. A. Abanin, L. S. Levitov, P. Kim, *Phys. Rev. Lett*. 2007, **99**, 186804
11. M. I. Katsnelson, K. S. Novoselov, A. K. Geim, *Nature Physics*, 2006, **2**, 620.
12. M. Han, B. Ozyilmaz, Y. Zhang, P. Jarillo-Herrero, P. Kim, *Phys. Status Solidi B Basic Solid State Phys*. 2007, **244**, 4134.
13. G. Eda, G. Fanchini, M. Chhowalla, *Nat. Nanotechnol*. 2008, **3**, 270.
14. K. C. Kwon, W. J. Dong, G. H. Jung, J. Ham, J.-L. Lee, S. Y. Kim, *Sol. Energy Mater. Sol. Cells*, 2013, **109**, 148.
15. T. H. Seo, J. -P. Shim, S. J. Chae, G. Shin, B. K. Kim, D. -S. Lee, Y. H. Lee, E. -K. Suh, *App. Phys. Lett*. 2013, **102**, 031116.
16. R. R. Nair, P. Blake, A. N. Grigorenko, K. S. Novoselov, T. J. Booth, T. Stauber, N. M. R. Peres, A. K. Geim, *Science* 2008, **320**, 1308.
17. L. A. Chernozatonskii, A. A. Artyukh, D. G. Kvashnin, *JETP Lett*. 2012, **95**, 266.
18. W. Kwon, S. Do, S. -W. Rhee, *RSC Adv*. 2012, **2**, 11223.
19. J. Shen, Y. Zhu, X. Yang, J. Zong, J. Zhang, C. Li, *New J. Chem*. 2012, **36**, 97.
20. V. Gupta, N. Chaudhary, R. Srivastava, G. D. Sharma, R. Bhardwaj, S. Chand, *J. Am. Chem. Soc*. 2011, **133**, 9960.
21. G. Eda, Y.-Y. Lin, C. Mattevi, H. Yamaguchi, H.-A. Chen, I.-S. Chen, C. -W. Chen, M. Chhowalla, *Adv. Mater*. 2010, **22**, 505.
22. J. K. Kim, M. J. Park, S. J. Kim, D. H. Wang, S. P. Cho, S. Bae, J. H. Park, B. H. Hong, *ACS Nano*, 2013, **7**, 7207.
23. D. H. Wang, J. K. Kim, J. H. Seo, I. Park, B. H. Hong, J. H. Park, A. J. Heeger, *Angew. Chem. Int. Ed*. 2013, **52**, 2874.
24. Y. Li, Y. Hu, Y. Zhao, G. Shi, L. Deng, Y. Hou, L. Qu, *Adv. Mater*. 2011, **23**, 776.
25. N. S. Sariciftci, L. Smilowitz, A. J. Heeger, F. Wudl, *Science* 1992, **258**, 1474.
26. G. Yu, J. Ga, J. C. Hummelen, F. Wudl, A. J. Heeger, *Science* 1995, **270**, 1789.
27. A. J. Heeger, *Angew. Chem. Int. Ed*. 2001, **40**, 2591.
28. T. -H. Han, Y. Lee, M. -R. Choi, S. -H. Woo, S. -H. Bae, B. H. Hong, J. -H. Ahn, T. -W. Lee, *Nat. Photon*. 2012, **6**, 105.
29. H. Kim, S. -H. Bae, T. -H. Han, K. -G. Lim, J. H. Ahn, T. -W. Lee, *Nanotechnology* 2014, **25**, 014012.
30. W. Kwon, Y. -H. Kim, C. -L. Lee, M. Lee, H. C. Choi, T. -W. Lee, S. -W. Rhee, Nano Letts. 2014, **14**, 1306
31. P. W. M. Blom, V. D. Mihailetchi, L. J. A. Koster, D. E. Markov, *Adv. Mater*. 2007, **19**, 1551.
32. M. J. Beliatis, K. K. Gandhi, L. J. Rozanski, R. Rhodes, L. McCafferty, M. R. Alenezi, A. S. Alshammari, C. A. Mills, K. D. G. I. Jayawardena, S. J. Henley, S. R. P. Silva, *Adv. Mater*. 2014, **26**, 2078.
33. H. B. Yang, Y. Q. Dong, X. Wang, S. Y. Khoo, B. Liu, C. M. Li, *Sol. Energy Mater. Sol. Cells* 2013, **117**, 214.
34. T. S. van der Poll, J. A. Love, T.-Q. Nguyen, G. C. Bazan, *Adv. Mater*. 2012, **24**, 3646.
35. A. K. K. Kyaw, D. H. Wang, D. Wnands, J. Zhang, T.-Q. Nguyen, G. C. Bazan, A. J. Heeger, *Nano Lett*. 2013, **13**, 3796.
36. A. K. K. Kyaw, D. H. Wang, V. Gupta, J. Zhang, S. Chand, G. C. Bazan, A. J. Heeger, *Adv. Mater*. 2013, **25**, 2397.
37. X. Li, W. C. H. Choy, L. Huo, F. Xie, W. E. I. Sha, B. Ding, X. Guo, Y. Li, J. Hou, J. You, Y. Yang, *Adv. Mater*. 2012, **24**, 3046.
38. D. H. Wang, D. Y. Kim, K. W. Choi, J. H. Seo, S. H. Im, J. H. Park, O O. Park, A. J. Heeger, *Angew. Chem. Int. Ed.* 2011, **50**, 5519 .
39. D. H. Wang, K. H. Park, J. H. Seo, J. Seifter, J. H. Jeon, J. K. Kim, J. H. Park, O O. Park, Alan J. Heeger, *Adv. Energy Mater*. 2011, **1**, 766.